Journal of Alloys and Compounds 509 (2011) 7618–7624

Contents lists available at ScienceDirect

Journal of Alloys and Compounds

journal homepage: www.elsevier.com/locate/jallcom

W-type hexaferrite nanoparticles: A consideration for microwave attenuation at wide frequency band of 0.5–10 GHz

Muhammad Javed Iqbal [a,*], Rafaqat Ali Khan [a], Shigeru Takeda [b], Shigemi Mizukami [c], Terunobu Miyazaki [c]

[a] Surface and Solid State Chemistry Laboratory, Department of Chemistry, Quaid-i-Azam University, Islamabad 45320, Pakistan
[b] Magnontech Ltd., 787-16 Juroken, Kumagaya, Saitama, 360-0846, Japan
[c] WPI Advanced Institute for Material Research, Tohoku University, 2-1-1 Katahira, 980-8577 Sendai, Japan

ARTICLE INFO

Article history:
Received 23 January 2011
Received in revised form 19 April 2011
Accepted 19 April 2011
Available online 28 April 2011

Keywords:
Permanent magnets
Chemical synthesis
Microstructure
Magnetic measurements
Microwave absorption

ABSTRACT

The static and dynamic magnetic properties of W-type hexaferrites are tuned to meet the requirements of wide band frequencies for attenuation of electromagnetic interference and microwave absorptions purposes. For this purpose, the W-type hexaferrite of entirely new composition of $BaCoZnFe_{16-2y}Al_yCe_yO_{27}$ ($y = 0$, 0.2, 0.4, 0.6, 0.8 and 1.0) has been synthesized by the chemical co-precipitation. The material is characterized using X-ray diffraction (XRD), scanning electron microscopy (SEM) and vibrating sample magnetometer (VSM). The complex permittivity ($\varepsilon_r = \varepsilon' - j\varepsilon''$) and permeability ($\mu_r = \mu' - j\mu''$) spectra are determined using Vector Network Analyzer (VNA) in a range from 0.5 GHz to 10 GHz. During this study, it is noticeable that the Al^{3+} and Ce^{3+} ions have considerable effect on the shape of the nanoparticles. Samples having Al–Ce contents $y = 0.2$ and $y = 0.4$ showed large values for magnetization (70.5 emu/g) and remanent magnetization (32.9 emu/g). In addition, more than 99% absorption (>−20 dB) is noted for this sample composition. Based on these results it is concluded that the microwave absorption characteristics of these compounds can be tuned for the required frequency by varying the thickness of the absorber. Due to this reason, potential employment of the synthesized nanoparticles for absorption of electromagnetic radiations at wide frequency band of 0.5–10 GHz has been proposed.

1. Introduction

Current advances in the gigahertz (GHz) electronic devices and equipments are bringing pleasing soothe to the human life on one hand but on the other hand creating some critical environmental problems. One of these problems is the electromagnetic interference (EMI) caused by malfunction of electronic devices. Since last few years, much attention has been devoted by researchers towards minimization of the EMI. Ferrites are ideal materials for EMI attenuation due to their dielectric and magnetic characteristics. Among ferrites, W-type Ba-hexaferrites are the most efficient compounds for microwave absorption purposes because of their highly tunable anisotropy field along the easy *c*-axis [1]. The criteria for the proposed material used as electromagnetic attenuation purposes, include two basic properties namely the complex permittivity and permeability at required frequencies [2]. For EMI attenuation purpose, the material should have large real and imaginary parts of permeability, and low value for the real part of permittivity together with the resonance frequency in microwave band [3].

Rare earth ions are known for their important role in the improvement of the electromagnetic absorption characteristics of ferrites at a wide frequency band. For example, substitution of Nd^{3+} on Ba^{2+} site in $BaCo_2Fe_{16}O_{27}$ resulted in a considerable increment of microwave absorption [4]. A reflection loss (RL) of 39.6 dB and absorption bandwidth of more than 8 GHz (at −10 dB) with matching thickness of 2 mm are obtained for La^{3+} doped W-type hexaferrite [5]. Similarly when La^{3+} was doped in M-type hexaferrite the reflection loss was −41.7 dB (at −10 dB) over 4 GHz at a thickness of 2.3 mm [6]. Er^{3+} in W-type hexaferrites minimized the reflection loss to a value of −27.4 dB (below −10 dB) with a matching thickness of 2.6 mm [7]. In addition, incorporation of some non-magnetic metal oxides such as $Sn_{0.9}Sb_{0.1}O_2$, improved the high frequency magnetic properties of W-type hexaferrites [8].

W-type hexaferrites have superior magnetic properties as compared to the other ferrites of similar crystal structure. Therefore doping with a suitable choice of dopants can vary their magnetic parameters for useful applications. Doping of $BaCd_2Fe_{16}O_{27}$ with Sr^{2+} ions on divalent Cd^{2+} sites an increase of 39% and 19% in the

* Corresponding author. Tel.: +92 51 90642143; fax: +92 51 90642241.
E-mail address: mjiqauchem@yahoo.com (M.J. Iqbal).

0925-8388/$ – see front matter © 2011 Elsevier B.V. All rights reserved.
doi:10.1016/j.jallcom.2011.04.103

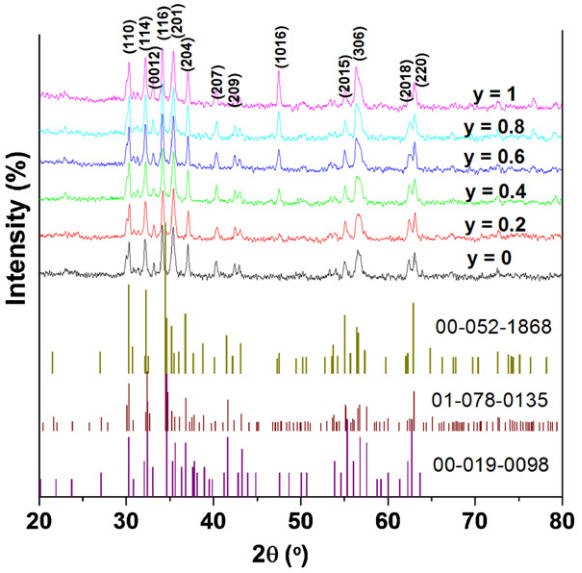

Fig. 1. XRD patterns of substituted $BaCoZnFe_{16-2y}Al_yCe_yO_{27}$ (y = 0–1) hexaferrites nanoparticles.

values of saturation magnetization and remanent magnetization, respectively, have been achieved [9]. Saturation magnetization of 67.0 emu/g and remanent magnetization of 34.7 emu/g are obtained for a Zr^{4+}–Mn^{2+} substituted W-type hexaferrites system [10].

Taking into consideration the required criterion for the development of microelectronics, we have attempted to synthesize Ba-W type hexaferrites nanoparticles. The basic skeleton selected for this purpose is $BaCoZnFe_{16}O_{27}$ because of its superior electromagnetic absorption characteristics at microwave frequencies [11]. The reason for selecting a combination of Al^{3+} and Ce^{3+} is that some of the previous investigations deal with rare earth ion substitution either on bivalent or trivalent ionic sites, e.g., on the site of Ba^{2+} [12,13] ions or on the Fe^{3+} site without any combination with other ions [14]. Therefore, these attempts mostly resulted in the formation of extra phases together with the compound of interest. Hence, small size Al^{3+} in combination with Ce^{3+} ions is used to replace Fe^{3+} at different sublattices of W-type crystal structure. Ce^{3+} belonging to rare earth family has unique relaxation characteristics and perhaps has some interesting effects on electromagnetic properties. Previously, the addition of Ce^{3+} ions in lithium ferrites on the iron site played an important role in the enhancement of electromagnetic attenuation characteristics [15]. Similarly, Al^{3+} ions are reported to modify the anisotropy field along the c-axis in M-type hexaferrites and hence have strong effect on magnetic properties [16]. To the best of our knowledge, the substitution of Al^{3+} and Ce^{3+} ions in W-type hexaferrites for the purpose of improving their magnetic and microwave properties has never been reported. Hence, study of the effect of substitution of these ions on the structural, magnetic and microwave properties would further help in understanding the W-type hexaferrites at nanometer scale.

2. Experimental

The chemical co-precipitation method was utilized to synthesize nanoparticles of the W-type hexaferrite doped with different contents, y, of Al–Ce binary mixture. $BaCoZnFe_{16-2y}Al_yCe_yO_{27}$ (where y = 0, 0.2, 0.4, 0.6, 0.8 and 1.0). The chemicals used for the synthesis includes barium nitrate (Fluka, 99%), cobalt acetate tetra-hydrated (Merck, 99%), zinc chloride (Aldrich, 98%), iron nitrate nona-hydrated (Merck, 98%), aluminium nitrate nona-hydrated (Merck, 95%), cerium nitrate hexa-hydrated (Sigma–Aldrich, 98%). Sodium hydroxide (Merck, 98%) and sodium carbonate (Merck, 99%) buffer was used as precipitating agent. During the synthesis process, mixing of stoichiometric amounts of the corresponding chemicals in distilled water formed a homogeneous mixture of solution. Under constant stirring, the solution temperature was enhanced to 353 K followed by drop wise addition of a mixture of sodium hydroxide and sodium carbonate in a ratio of 5:1 to raise the solution pH up to 11 at which the precipitates started to appear. The precipitates washed 3–4 times with distilled water and dried at a temperature of 373 K. The granules were grinded to a powder form and finally annealed for 4 h at 1153 K at a heating rate of 5 K min^{-1} using a temperature programmed tube furnace. The synthesized nanoparticles powder was characterized using a diffractometer (SmartLab by Rigaku Corp.) that employs CuK_α as a radiation source. For microstructure analysis, we made use of scanning electron microscope (Hitachi S-3400N). Room temperature static magnetic properties were studied using vibrating sample magnetometer (Model: VSM-5-15 AUTO by Toei Kogyo Co. Ltd. Tokyo, Japan). For permittivity measurement, the sample having dimension of 5 mm × 1.9 mm × 0.5 mm (±0.05 mm) were placed close to the reference plane in a test fixture during measurement method known as "open ended strip line method". The transmission line having 50 Ω impedance was used during measurements. The all shielded shorted microstrip line method was used to measure complex permeability with E 8362B Agilent Technologies PNA series network analyzer (E 8362B). The detail of the measurement can be found elsewhere [17]. During the measurement, a square slab, having dimensions 5 mm × 5 mm × 0.5 mm (±0.05) (device under test, DUT) was closely inserted and fixed to the short end while static magnetic field was applied across the specimen. Errors due to the residual parameters of the test fixture were minimized effectively by performing OPEN, SHORT and known LOAD calibrations on the DUT contact surface of the test fixture.

3. Results and discussion

3.1. Phase identification (XRD) and microstructure (SEM)

The powdered X-ray diffraction patterns given in Fig. 1 indicate the crystal structure of W-type hexaferrites which perfectly match with the standard patterns for pure $BaCo_2Fe_{16}O_{27}$ (00-0019-98, 01-078-0135) and pure $BaZn_2Fe_{16}O_{27}$ (00-052-1868). It is found that the crystal structure is retained upon doping with high levels of substitution, i.e., y = 1.0 although further substitution was not attempted because of possibility of deterioration of magnetic properties. The lattice constants 'a' and 'c' shown in Table 1, are calculated using equation:

$$\frac{1}{d_{hkl}^2} = \frac{4(h^2 + hk + k^2)}{3a^2} + \frac{l^2}{c^2}$$

Table 1
Structural parameters (XRD), magnetic parameters calculated from M–H loops and values for peak absorption, reflection loss, and bandwidths for all compositions.

Al–Ce content, y	0	0.2	0.4	0.6	0.8	1
Lattice constant, a (Å)	5.855	5.864	5.867	5.871	5.865	5.876
Lattice constant, c (Å)	33.17	33.25	33.30	33.39	33.43	33.51
Crystallite sizes, D (nm)	37	34	37	40	38	38
[a]Magnetization, M_{15} (emu/g)	65.3	67.1	70.5	63.1	61.1	60.8
Remenant magnetization, M_r (emu/g)	28.1	29.0	32.9	29.9	28.6	29.1
Coercivity, H_c (kOe)	1.31	1.17	1.27	1.34	1.36	1.55
t (mm)	4.90	3.85	4.59	4.66	4.85	4.94
Peak value f_m (GHz)	8.27	7.97	8.52	8.27	8.07	7.77
Peak value, R_L (dB)	−19.2	−29.1	−22.5	−17.6	−19.9	−17.9
Band width at −10 dB (GHz)	1.98	1.38	1.78	1.58	1.82	1.37

[a] Room temperature magnetization at 15 kOe.

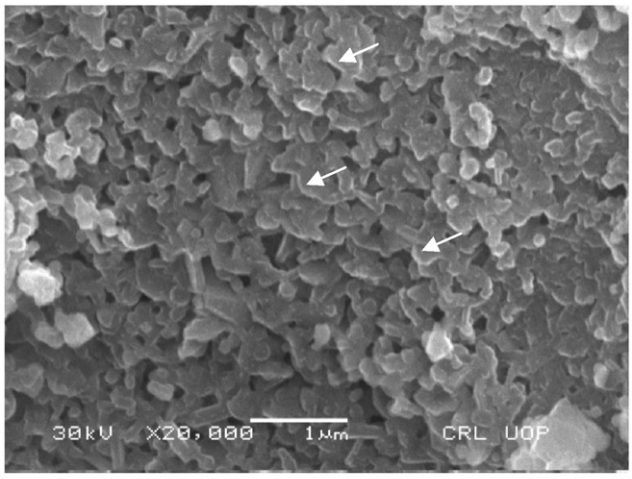

(a) y = 0

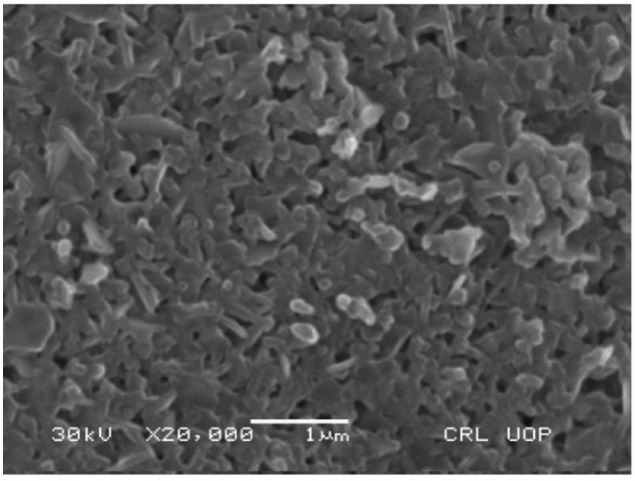

(b) y = 0.2

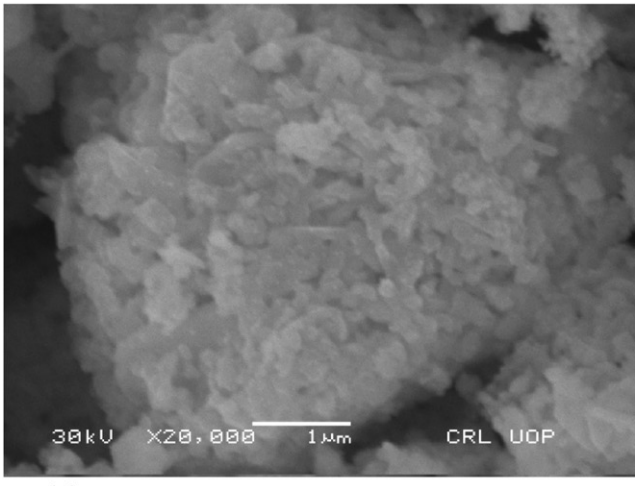

(c) y = 1.0

Fig. 2. Scanning electron microscope images for (a) $BaCoZnFe_{16}O_{27}$, (b) $BaCoZnFe_{15.6}Al_{0.2}Ce_{0.2}O_{27}$ and (c) $BaCoZnFe_{14}AlCeO_{27}$.

where *h*, *k* and *l* are Miller indices and *d* is the inter planer spacing. It is clear from the table that the value of '*a*' remains almost constant while that of '*c*' increases slightly due to large ionic radius of Ce^{3+}(1.11 Å) as compared to that of Fe^{3+} (0.64 Å). On the other hand, Al^{3+} (0.53 Å) compensates for the addition of larger rare earth ion so that to protect the formation of extra phases as is evident from the XRD patterns. Previously M-type hexaferrites (Both Ba- and Sr-M type) were doped with Al^{3+} [18]. It was found that almost half of the iron sites of $BaFe_{12-x}Al_xO_{19}$ could be replaced with Al^{3+} without distortion of hexagonal structure. On the other hand, $SrFe_{12-x}Al_xO_{19}$ can be produced with any content of aluminium up to complete replacement of iron. The reason is small size of Al^{3+} compared to that of Fe^{3+}. Although for cerium substituted ferrites some extra phases are formed at higher dopant concentration because of large ionic radius of Ce^{3+} [14]. Moreover, Ce^{3+} ions when substituted alone in alloys designed for hydrogen storage materials, enhance the formation of $La(La,Mg)_2Ni_9$ phase [19]. The increase in lattice constants is not as large as one can expect from the addition of large Ce^{3+} ion and the reason for this is to the large binding energy of rare earth ions at octahedral sites [20]. The crystallite sizes of the samples are calculated from full width at half maximum (FWHM) of the reflections in the XRD pattern using Debye Scherrer formula ($D = k\lambda/\beta \cos\theta_B$), where k (0.89) is the shape constant, β is the broadening of diffraction line measured at half width of maximum intensity and λ is the X-ray wavelength used for the analysis, i.e. (1.542 Å). The calculated crystallite sizes are found to be in the range of 33–42 nm and are given in Table 1.

Fig. 2(a)–(c) shows the micrographs for the having different dopant contents, i.e. $y = 0$, $y = 0.2$ and $y = 1.0$, respectively, indicating the coagulated nanoparticles with a uniform size distribution. Inspection of Fig. 2(a) reveal that for $y = 0$ the particles exhibit a plate-like shape with more or less sharp edges, indicated by arrows in the micrograph. However, the scanning electron microscopy (SEM) patterns change when dopant level of $y = 0.2$ is substituted (Fig. 2b).The particles become elongated with the reduction of sharpness at the edges. With further addition of Al^{3+} and Ce^{3+} the particles continue to grow until the dopant concentration is $y = 1.0$. The particles become granular in shape as can be seen clearly in Fig. 2(c). Finally, it may be argued that in addition to strong effects related to electrical and magnetic behavior the doped Al^{3+} and Ce^{3+} ions show remarkable contribution to the morphology of the materials.

3.2. Magnetic characterization

M–H loops for Al–Ce substituted $BaCoZnFe_{16-2y}Al_yCe_yO_{27}$ compound prepared with different contents $y = 0, 0.2, 0.4, 1.0$ are plotted in Fig. 3. Table 1 summarizes the corresponding values for magnetization measured at 15 kOe (M_{15}), remanent magnetization (M_r) and coercivity (H_c) for all the synthesized samples. It is clear that both M_{15} and M_r increase up to a content of $y = 0.4$ to maximum and after that continuously decrease and to even less than the values for the undoped composition. Relatively lower concentration of $y = 0.2$ exhibits a minimum value of H_c but with further addition of Al–Ce content the value of H_c is enhanced to approach a maximum value. The structure of W-type hexaferrite consists of S-block, i.e., spinel block, and R-block containing large divalent Ba ions. These blocks arrange themselves together in such a manner along the *c*-axis to form repeated structure of *RSSR*S*S** [4]. The various octahedral and tetrahedral sites in these blocks contain seven different types of sublattices, occupied by various cations [21]. Positions of these ions strongly affect the electrical as well as magnetic properties of W-type hexaferrites. For getting a clear idea, the number, coordination, and the spin orientation of various cationic sublattices are shown in Table 2. In case of M-type hexaferrites, it has been previously reported that Al^{3+} prefer tetrahedral f_{IV}, and octahedral 2a, 12k sites [22,23]. Considering the analogy between the structure of M-type and W-type hexaferrites it could be assumed that at lower concentrations Al^{3+}, with magnetic moment of $\mu_B = 0$, would occupy tetrahedral 4e and $4f_{IV}$ site. From Table 2, it is clear that these sublattices have spin down geometry. Therefore, due to

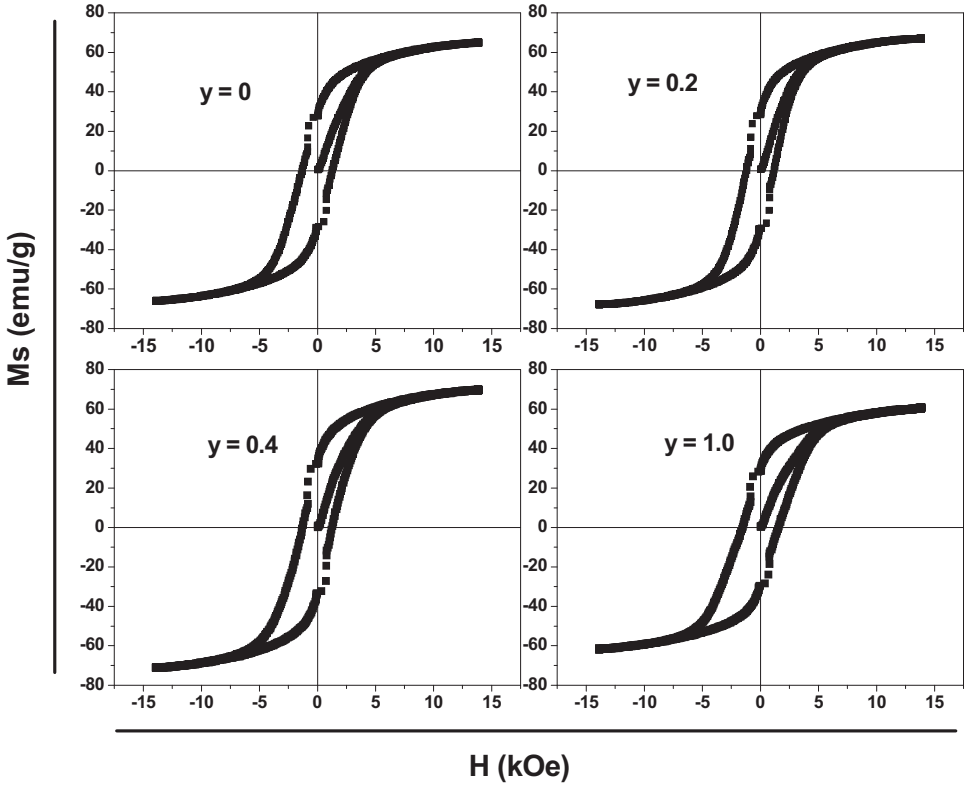

Fig. 3. Hysteresis loops for selected $BaCoZnFe_{16-2y}Al_yCe_yO_{27}$ ($y = 0$, 0.2, 0.4, 0.6, 0.8, and 1.0).

Al^{3+} substitution at these sites, the resultant spin along the easy direction can get increased and the resultant effect on overall magnetization is positive. On the other hand, Ce^{3+} with 4*f* electrons have some magnetic moment [24]. Due to its ionic size, probably it may occupy one of the octahedral sites with spin up direction along the *c*-axis. In both these cases whether Ce^{3+} occupy sublattice having an electronic spin up or spin down, the doping results in decrease of M_{15} and M_r values. Moreover, the spin canting effect (in which the orientation of magnetic ions align by making angles from the preferred direction) usually caused by the rare earth ions, also suppresses the exchange interaction strength and thus promotes the lower M_{15} value. Therefore due to the reasons mentioned above, the combined doping of Al^{3+} and Ce^{3+} increases the room temperature magnetization up to their content of $y = 0.4$. After that, M_{15} decreases due to the diamagnetic nature of Al^{3+} ions, which weakens the super exchange interactions among sublattices.

The coercivity of the material depends upon the anisotropic field the porosity and the particle size of the material. Inspection of SEM images for compositions having $y = 0$ (Fig. 2a) and $y = 0.2$ (Fig. 2b), shows that the undoped sample ($y = 0$) contain higher number of pores as compared to that of the doped samples. It is understood that when the number of pores is high, average particle size would be smaller and the value of coercivity for the material would be high as compared to the non-porous material. This assumption holds well if we look at the values of coercivities for the sample with the dopant contents of $y = 0$ and $y = 0.2$ as shown in Table 1. Further increase in the value of coercivity can be correlated to the effect of substituent particularly Al^{3+} ions. Previously, it was reported that Al substituted M-type hexaferrite show large coercivities due to its ability to increase the anisotropy field [25,26]. On the other hand, the rare earth ions are also reported to increase the magneto crystalline anisotropy of the material [27]. Therefore, in our case the increase in the coercivity value with the addition of dopant is due to the increase in the anisotropy along *c*-axis, which is the easy axis of magnetization in W-type hexaferrites.

3.3. Complex relative permittivity and permeability spectra

Fig. 4(a)–(f) shows the complex relative permittivity ($\varepsilon_r = \varepsilon' - j\varepsilon''$) and complex relative permeability ($\mu_r = \mu' - j\mu''$) spectra for different compositions of W-type hexaferrites having both real and imaginary parts in the range from 0.5 GHz to 10 GHz. By critical analysis of these data one can notice that the real part of permittivity (ε') for the compositions $y = 0.2$ (Fig. 4b) and $y = 0.4$ (Fig. 4c) remains almost constant in the entire range of measurements between 0.5 GHz and 10 GHz. While for other compositions the real part of permittivity slightly decreased as the frequency increases up to 10 GHz. Furthermore the data show that the average value for the real part of permittivity in case of the composition $y = 0.6$ (Fig. 4d) is high while for the composition

Table 2
Number of ions, coordination, spin orientations and the occupying blocks for M-type and W-type hexaferrites.

Sublattices (M-type)	12k	f_{IV}		f_{VI}	2a		2b
(W-type)	12k	4e	$4f_{IV}$	$4f_{VI}$	6g	4f	2d
Coordination	Octa	Tetra	Tetra	Octa	Octa	Octa	Bi-pyramidal
No. of ions	6	2	2	2	3	2	1
Blocks	R-S	S	S	R	S-S	S	R
Spin	Up	Down	Down	Down	Up	Up	Up

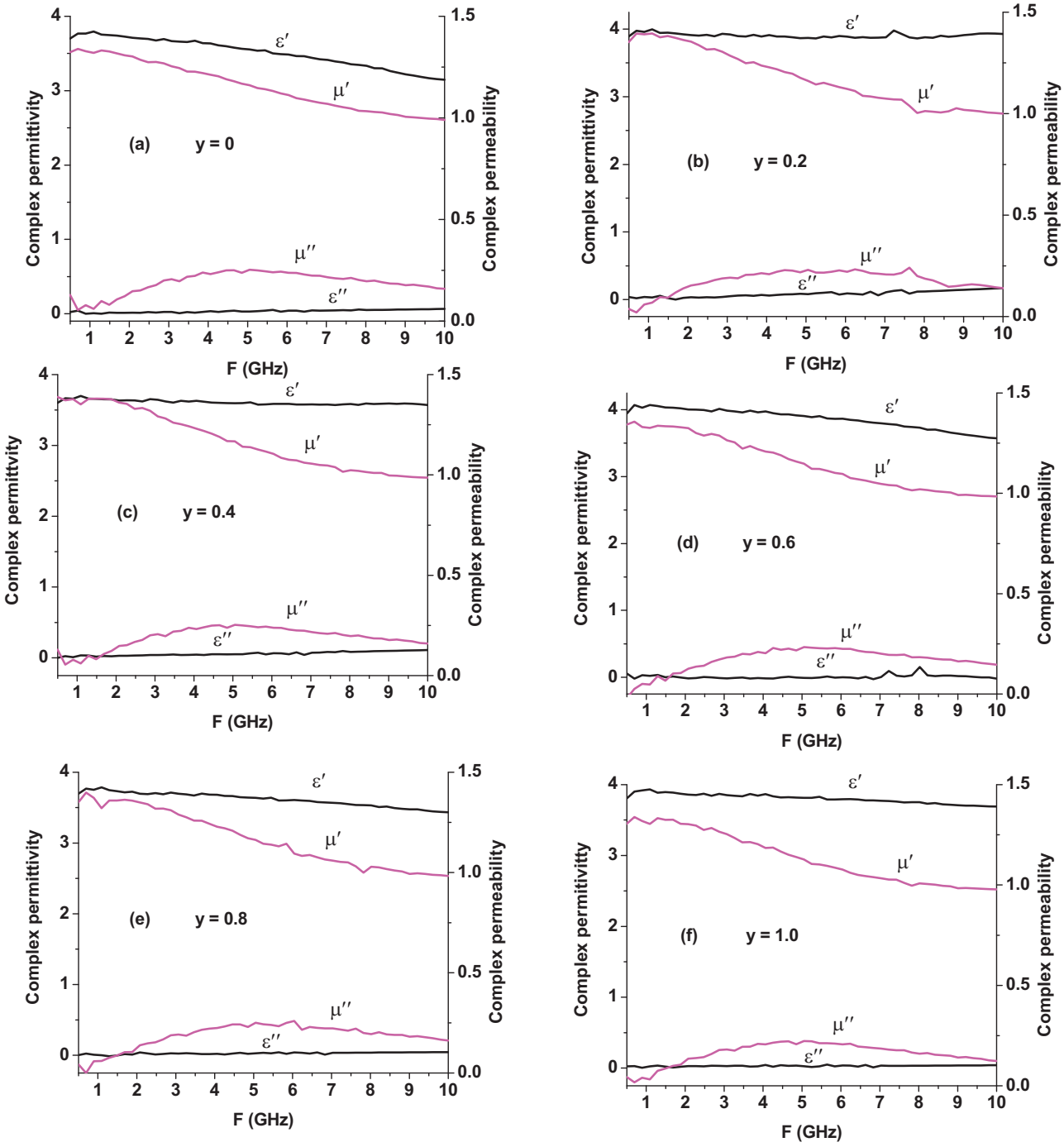

Fig. 4. Complex relative permittivity and complex relative permeability for $BaCoZnFe_{16-2y}Al_yCe_yO_{27}$ (y = 0–1.0) hexaferrites nanoparticles.

y = 0.4 (Fig. 4c) it is the lowest. The imaginary part of permittivity on the other hand remains very low with value of less than 0.01 in all cases.

The value of permittivity for the ferrites at high frequencies mainly depends upon the atomic and electronic polarization with in the ceramic grains. The affect relating to the substitution of iron for a combined addition of Al^{3+} and Ce^{3+} ions is twofold. First at lower concentration up to y = 0.4, it reduces the overall concentration of iron ions in a material under study, which in turn lowers the possibility of electronic hopping between a pair, of Fe^{3+} and Fe^{2+}. In this pair, the Fe^{2+} ion with an extra electron is more polarizable as compared to Fe^{3+} having half filled d-orbital with spherical symmetry. This phenomenon is responsible for large values of permittivity and reduced iron ion concentration resulting in the observed low average value for ε' (Fig. 4c). The second outcome of the dopants, especially Ce^{3+}, is the possibility of transformation to the tetravalent (Ce^{4+}) ionic form and thus stands responsible for the conversion of some of Fe^{3+} to Fe^{2+} beyond a certain concentration. Fig. 4(d) shows that for the permittivity spectra for y = 0.6 this assumption holds good. In addition, the microstructure, i.e., shape of the particles and porosity, have also affects the polarization processes. The addition of Al^{3+} and Ce^{3+} have considerable effect on the microstructure of the material as discussed in Section 3.1. Therefore all these contributions account for the monotonous behavior

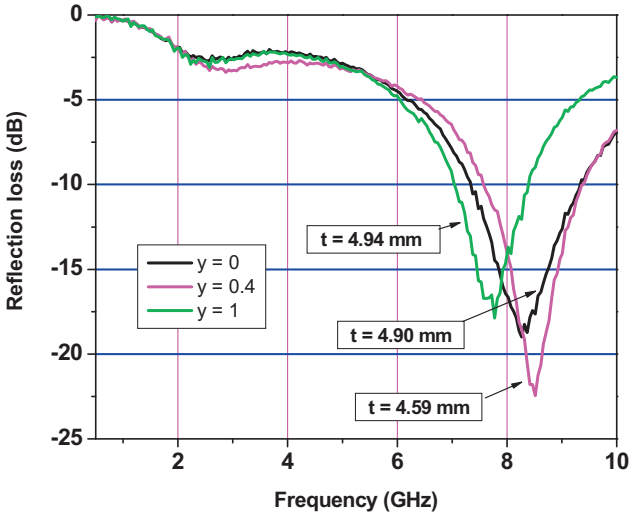

Fig. 5. Microwave absorption characteristics for $BaCoZnFe_{16-2y}Al_yCe_yO_{27}$ ($y = 0$, 0.4, 1.0) at optimum absorber thickness values.

of ε' observed for the compositions $y = 0.2$ and $y = 0.4$ as shown in Fig. 4(b) and (c), respectively.

Along with the permittivity, the complex relative permeability ($\mu_r = \mu' - j\mu''$) spectra of samples with different contents of Al^{3+} and Ce^{3+} are shown in Fig. 4(a)–(f). These spectra depict that the real part of complex relative permeability, μ', continuously decreases in the measured frequency range of 0.5 GHz to 10 GHz and this trend becomes more prominent below 8 GHz. There is not much difference in the average values for the real part of complex permeability (μ') but have large average values of μ' for a content of $y = 0.2$ (Fig. 4b) and $y = 0.4$ (Fig. 4c). Imaginary part of complex permeability (μ'') shows a broad and relatively weak frequency dispersion phenomenon for of the all samples under investigation. Another most interesting behavior is evident from Fig. 4(b) and (e). In Fig. 4(b) ($y = 0.2$) there is a relatively small dispersion peak at ~7.5 GHz for both ε_r and μ_r while in Fig. 4(e) ($y = 0.8$) in addition to 7.5 GHz there is an extra peak at ~6 GHz for μ_r.

The decrease in the real part of permeability at higher frequencies above 4 GHz is a normal behavior for the ferrites, which is due to the limited speed of spin and domain wall moment [28]. This phenomenon contributes positively to the matching of microwave surface impedance because as the frequency goes towards high values, the wavelength in microwave absorber decreases [29]. Generally, it is normal for the magnetic materials of higher room temperature magnetization and higher permeabilities. As discussed in Section 3.2 and also clear from M_{15} values given in Table 1 that the samples studied here having dopant contents of $y = 0.2$ and $y = 0.4$ show maximum room temperature magnetizations. Therefore, the observed large values of μ' for these samples are due to the enhancement of resultant magnetic moments along the *c*-axis. The broad absorption peaks for all the samples studied here in a range of 2–7 GHz is perhaps due to the presence of both natural resonance and wall resonance simultaneously and are characteristics of polycrystalline ferrites [30]. The anomalous behavior of samples having Al–Ce contents of $y = 0.2$ and $y = 0.8$ at frequencies of 6 GHz and 7.5 GHz are perhaps due to the relaxation phenomenon associated with the rare earth ion Ce^{3+}. However, the occurrence of these peaks requires further more detailed investigations.

3.4. Microwave absorption

The predictions of the transmission line the theory [29] underline the reflection coefficient (dB) as a function of normalized input

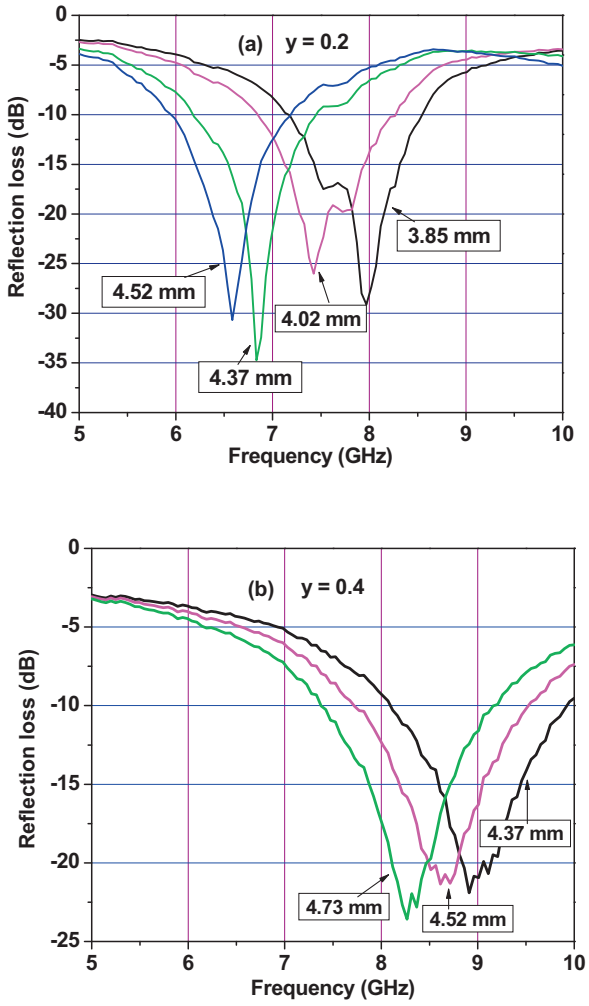

Fig. 6. Dependence of the reflection loss (*RL*) on thickness (*tm*) of the absorber for sample (a) $BaCoZnFe_{15.6}Al_{0.2}Ce_{0.2}O_{27}$ ($y = 0.2$) and (b) $BaCoZnFe_{15.2}Al_{0.4}Ce_{0.4}O_{27}$ ($y = 0.4$).

impedance at the surface of a single layer material backed by conductor and is given by following equation.

$$R_L = -20 \log_{10}\left[\frac{Z_{in} - Z_0}{Z_{in} + Z_0}\right] \quad (1)$$

where Z_0 denotes the characteristic impedance of free space and given by

$$Z_0 = \sqrt{\frac{\mu_0}{\varepsilon_0}} \quad (2)$$

Z_{in} is the input impedance at the air-absorber interface and is represented by

$$Z_{in} = Z_0\sqrt{\frac{\mu_r}{\varepsilon_r}}\tanh\left[\left(-j\frac{2\pi ft}{c}\right)\sqrt{\mu_r\varepsilon_r}\right] \quad (3)$$

where $\mu_r = \mu' - j\mu''$ and $\varepsilon_r = \varepsilon' - j\varepsilon''$ are the complex relative permeability and permittivity, respectively, for the absorber medium, *f* is the frequency, *c* is the velocity of light and *t* is the thickness of samples. The conditions for impedance matching at which Z_{in} becomes equal to Z_0 are satisfied at particular matching thickness (t_m) and matching frequency (f_m). The matching thickness is expressed by the following equation

$$t_m = \frac{\lambda_a}{4} = \frac{c}{4f_0\sqrt{\mu_r\varepsilon_r}} \quad (4)$$

Table 3
Peak absorption, and band width observed at various thicknesses for $BaCoZnFe_{16-2y}Al_yCe_yO_{27}$ ($y = 0.2, 0.4$).

t (mm)	Peak value (GHz)	Peak value, R_L (dB)	Band width (GHz)
($y = 0.2$)			
3.85	7.97	−29.13	1.38
4.02	7.43	−26.02	1.44
4.37	6.83	−34.73	1.27
4.52	6.58	−30.68	1.25
($y = 0.4$)			
4.37	8.91	−21.90	1.82
4.52	8.61	−21.35	1.82
4.73	8.27	−23.57	1.79

where λ_a is the wavelength inside the absorber, f_0 is the incident frequency of free space. This equation shows that when the thickness of absorber is equal to one quarter of wavelength, the wave reflected at the air–absorber interface is out of phase with the wave reflected at absorber–metal interface.

Reflection loss (R_L) values for some of the samples having different Al–Ce contents in their composition, as calculated by Eqs. (1)–(3), lie between 0.5 GHz and 10 GHz (see Fig. 5). The reflection loss (R_L) is measured at the optimum values of the matching thickness (t_m) [31]. The figure shows a minimum reflection loss of −22.5 dB for the sample having Al–Ce content, $y = 0.4$ at an optimum thickness of 4.59 mm with peak value at 8.5 GHz. All the synthesized samples show greater than 90% absorption with various matching thicknesses. In some cases as for compositions with Al–Ce contents of $y = 0.2$ (Fig. 6a) and $y = 0.4$ (Figs. 5 and 6b) more than 99% of absorption is achieved. Table 1 shows the peak absorption values and absorption bandwidths for the samples along with the values of the optimum thickness. It is clear from the table that the peak value for maximum absorption at the optimum thickness shifts towards the lower frequency with increase in the dopant content, y. The maximum absorption which is more than 99% in case of $y = 0.2$ and $y = 0.4$ is due to the lowering of permittivity and corresponding increase in the permeability. This phenomenon is responsible for fulfilling the matching conditions for the impedance of $Z_{in} = Z_0$. As it is obvious, that for achieving matching conditions for the impedance, the complex permittivity, and complex permeability are tuned so that their values are comparable to each other. This requirement should stand responsible for the prevention of any front surface reflections from the material layer. Although dielectric loss is negligibly small in the measured frequency range but the magnetic loss is so appreciable that it converts the incoming electromagnetic waves in to heat by interacting with them. Fig. 6(a) shows the R_L values calculated for the sample with composition $y = 0.2$ at different values of t_m.The figure shows an interesting trend that the R_L minima is shifted towards lower frequency by increasing absorber thickness (t_m). The same phenomenon was observed previously in case of U-type hexaferrites [31]. In case of the spectra for $t_m = 3.85$ and $t_m = 4.02$, there are small peaks besides large absorption due to the anomalies in the measured values of the complex permittivity and complex permeability for composition contains dopant contents of $y = 0.2$ at 7.5 GHz. Table 3 indicates that this sample has more that 99.5% absorption for the selected t_m values and at the same time show variations in the absorption bandwidths. Similarly Fig. 6(b) shows the variations of microwave absorption for the dopant substitution level of $y = 0.4$, at different thicknesses. Although in this case, maximum absorption is attained at a matching thickness $t_m = 4.73$ mm the bandwidth is slightly decreased (Table 3) as compared to that of observed at $t_m = 4.37$ mm. The same trend is observed for all the other samples, which indicates the tunability of these materials by only changing the thickness of the absorbers. Therefore, these materials can be employed for electromagnetic attenuations purposes and as radar absorbing materials at the GHz frequency range in order to reduce the radar cross section area.

4. Conclusions

Substitution of a combination of Al^{3+} and Ce^{3+} in to the $BaCoZnFe_{16}O_{27}$ nanoparticles exhibits extraordinary properties relating to the magnetic and electromagnetic absorption characteristics. The variations in the values of M_{15}, M_r and H_c at different substitution levels of $Al^{3+} + Ce^{3+}$ ions guarantee the potential usage of these materials as permanent magnets in various electrical devices. The microstructure of the synthesized material is also affected significantly by the substitutions. Hence, together with the absorption characteristics especially those shown by samples having content $y = 0.2$ and $y = 0.4$, these materials exhibit tunable characteristics with the variation of $Al^{3+} - Ce^{3+}$ contents. Moreover, shift in the frequency at which minimum reflection loss occurs is dependent on the thickness of the absorber. These characteristics show that Al–Ce doped W-type hexaferrite could be used for any desirable frequency. Owing to all these distinguished characteristics at higher frequencies, these materials are a potential candidate for attenuation of the electromagnetic interference and as radar absorbing materials.

Acknowledgment

The authors are thankful to Higher Education Commission (HEC) of Pakistan for supporting this work.

References

[1] R.S. Meena, S. Bhattachrya, R. Chatterjee, J. Magn. Magn. Mater. 322 (2010) 1923–1928.
[2] V. Sunny, P. Kurian, P. Mohanan, P.A. Joy, M.R. Anantharaman, J. Alloys Compd. 489 (2010) 297–303.
[3] Y.P. Wu, C.K. Ong, G.Q. Lin, Z.W. Li, J. Phys. D: Appl. Phys. 39 (2006) 2915–2919.
[4] J. Xu, H. Zou, H. Li, G. Li, S. Gan, G. Hong, J. Alloys Compd. 490 (2010) 552–556.
[5] L. Deng, L. Ding, K. Zhou, S. Huang, Z. Hu, B. Yang, J. Magn. Magn. Mater. 323 (2011) 1895–1898.
[6] N. Chen, K. Yang, M. Gu, J. Alloys Compd. 490 (2010) 609–612.
[7] H. Xiaogu, Z. Jing, W. Hongzhou, Y. Shaoteng, W. Lixi, Z. Qitu, J. Rare Earth 28 (2010) 940–943.
[8] X. Huang, J. Chen, J. Zhang, L. Wang, Q. Zhang, J. Alloys Compd. 506 (2010) 347–350.
[9] G.M. Rai, F. Aen, M.U. Islam, M.U. Rana, J. Alloys Compd. 509 (2011) 4793–4796.
[10] M.J. Iqbal, R.A. Khan, S. Mizukami, T. Miyazaki, J. Magn. Magn. Mater. (2011), doi:10.1016/j.jmmm.2011.03.009.
[11] Y.J. Kim, S.S. Kim, IEEE Trans. Magn. 38 (2002) 3108–3110.
[12] L. Wang, J. Song, Q. Zhang, X. Huang, N. Xu, J. Alloys Compd. 481 (2009) 863–866.
[13] M.A. Ahmad, N. Okasha, R.M. Kershi, Physica B 405 (2010) 3223–3233.
[14] N. Rezlescu, C. Doroftei, E. Rezlescu, P.D. Popa, J. Alloys Compd. 451 (2008) 492–496.
[15] C. Sun, K. Sun, Solid State Commun. 141 (2007) 258–261.
[16] M.A. Popvo, I.V. Zavislyak, A.S. Tatarenko, G. Srinivasan, A.M. Balbashov, IEEE Trans. Magn. 45 (5) (2009) 2053–2058.
[17] S. Takeda, H. Suzuki, J. Magn. Soc. Jpn. 33 (2009) 171–174.
[18] N.J. Shirtcliffe, S. Thompson, E.S. O'Keefe, S. Appleton, C.C. Perry, Mater. Res. Bull. 42 (2007) 281–287.
[19] H. Pan, Q. Jin, M. Gao, Y. Liu, R. Li, Y. Lei, J. Alloys Compd. 373 (2004) 237–245.
[20] M.J. Iqbal, Z. Ahmad, J. Power Sources 179 (2008) 763–769.
[21] G. Albanese, M. Carbucicchio, G. Asti, Appl. Phys. 11 (1976) 81–88.
[22] G. Albanese, J. Magn. Magn. Mater. 147 (1995) 421–426.
[23] P. Singh, V.K. Babbar, A. Razdan, S.L. Srivastava, R.K. Puri, Mater. Sci. Eng. B 67 (1999) 132–138.
[24] C.J. Li, J.N. Wang, Mater. Lett. 64 (2010) 586–588.
[25] K. Haneda, H. Kojima, Jpn. J. Appl. Phys. 12 (1973) 355–360.
[26] G. Albanese, A. Deriu, Ceram. Int. 5 (1979) 3–10.
[27] J.F. Wang, C.B. Ponton, I.R. Harris, J. Alloys Compd. 403 (2005) 104–109.
[28] R.S. Meena, S. Bhattachrya, R. Chatterjee, J. Magn. Magn. Mater. 322 (2010) 2908–2914.
[29] Y. Yang, B. Zhang, W. Xu, Y. Shi, N. Zhou, H. Lu, J. Magn. Magn. Mater. 265 (2003) 119–122.
[30] Y.P. Wu, C.K. Ong, Z.W. Li, L. Chen, G.Q. Lin, S.J. Wang, J. Appl. Phys. 97 (2005) 063909-1–063909-6.
[31] R.S. Meena, S. Bhattachrya, R. Chatterjee, Mater. Des. 31 (2010) 3220–3226.